Conformational stability at low temperatures using single protein nanoaperture optical tweezers

Keiran Letwin, Matthew Peters & Reuven Gordon

2025

Conformational stability at low temperatures using single protein nanoaperture optical tweezers

Keiran Letwin,[†,‡] Matthew Peters,[*,†,‡] and Reuven Gordon[*,†,‡]

†*Department of Electrical Engineering, University of Victoria, Victoria, V8W 2Y2, British Columbia, Canada*

‡*Center for Advanced Material & Related Technologies, University of Victoria, Victoria, V8W 2Y2, British Columbia, Canada*

E-mail: rgordon@uvic.ca; rgordon@uvic.ca

Abstract

Nanoaperture optical tweezers allow for trapping single proteins and detecting their conformational changes without modifying the protein; i.e., being free from labels or tethers. While past works have used laser heating as a way to vary the local temperature, this does not allow for probing lower temperature values. Here we investigate the lower temperature dynamics of individual Bovine Serum Albumin (BSA) proteins, with the help of a custom peltier cooling stage. The BSA transitions between the normal (N) and fast (F) states. The normal form of BSA has a maximum occupancy at 21±1°C, which is interpreted as its maximum stability point for the compact N form with respect to the F form. In this way, it is possible to find the relative thermodynamic parameters of single proteins without requiring any modifications to the intrinsic structure.

Introduction

Nanostructured metals allow for extreme sensitivity in sensing, even at the single protein level.[1–4] They also experience Ohmic losses that can be used to locally heat and sometimes enhance the sensitivity of detection.[1] While many works have focused on plasmonic particles, and their heating capability,[5–7] nanoapertures have the advantage of conducting heat away due to the surrounding metal film. As a result, the heating is four orders of magnitude lower so laser powers suitable for trapping can be used without experiencing damaging temperature increases.[8]

Nanoaperture optical tweezers (NOTs) have been used to trap single proteins and other nanoparticles.[2,9–27] Several groups have investigated the thermal characteristics of NOTs,[28–32] where values of the order of a degree Kelvin per milliWatt are typical. Recently, the laser power variations have been used to change the local temperature in the trap and probe the changes in protein structure.[22,33] While this allows for exploring the temperature ranges close to physiological temperatures and above, the approach has not been used to probe

lower temperatures.

Here, we introduce a home-built cooling stage to the NOT trapping setup for accessing lower temperature values. The cooling stage uses a phase change material to effectively remove heat, and so it does not require moving fluids or fans that can affect the stability of the setup. This is desirable because the NOT requires sensitive alignment of the focused laser beam. Following our recent publication,[33] here we study the dynamics of Bovine Serum Albumin (BSA) at low temperatures, mapping out the transitions of the normal (N) state to fast (F) state with variations in temperature. We find the maximum occupancy of the N state and attribute this to the maximum stability of that state. The thermodynamics properties of single proteins can be explored in this way.

Past work has investigated the stability of BSA as a function of temperature,[34] following the Gibbs-Helmholtz equation:[35]

$$\Delta G(T) = \Delta H_{vF}\left(1 - T/T_m\right) - \Delta C_p\left((T_m - T) + T\ln\left(T/T_m\right)\right) \tag{1}$$

where T_m is the unfolding temperature, ΔH_{vF} and ΔC_p are the changes in van't Hoff enthalpy change and heat capacity change. This approach assumes a two-state transition, from folded to unfolded.[35] For BSA, it was found that the corresponding parameters are with T_m = 338.2K, ΔH_{vF} = 31kcal/mol and ΔC_p = 1.0 kcal/(K mol).[34] Using these parameters gives a maximum stability at 36°C. BSA, however, undergoes significant structural changes above 30°C,[36] and so the validity of the two-state model is questionable.

In our past work, the transition from F to the extended (E) state was found at higher powers.[33] Comparing the change in Gibbs free energy between those states (in that work Supplementary Figure 6),[33] we saw maxima at 38°C and 39°C for labeled and unlabeled versions of BSA. Those values show reasonable agreement with the expected result from the Helmholtz-Gibbs curve of 36°C, while ignoring the N state. Here we investigate instead the N to F transition and find the temperature at which the compact N state is most stable

relative to the F state.

NOT at Low Temperatures

Figure 1 shows the experimental setup and nanofabricated double nanohole (DNH) samples. It also shows the home-built cooling stage, with details in the Methods section below. Briefly, an 850 nm laser is focused on the DNH with a 100× oil immersion objective. The DNH was adjacent to the protein sample in a microwell chamber, and the transmitted light through the DNH was collected with another objective on the other side and detected using an avalanche photodiode (APD). When trapping occurs, there is a substantial increase in the APD voltage fluctuations due to the protein moving in the aperture and changing the transmission of light via scattering. There are also steps in the transmission level as the protein transitions between conformations. This was confirmed previously for BSA by forcing it into the E form with reduced pH.[2]

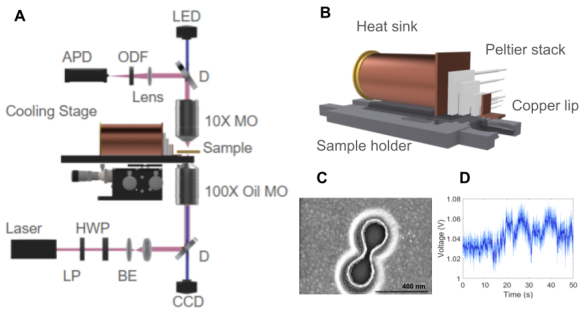

Figure 1: a)Schematic of NOT setup: LP = linear polarizer, HWP = half waveplate, BE = beam expander, CCD = charge coupled device, D = dichroic mirror, OI MO = oil immersion microscope objective, L = lens, ODF = optical density filter, APD = avalanche photodiode) SEM image of DNH. b) Schematic of cooling stage. A copper cylinder containing phase change material (palm-parrafin wax) serves as heat sink to a three peltier stack, connected to the top of the microscope slide sample with a copper bridging lip. c) SEM image of DNH in gold film (scale bar is 400 nm). d) APD voltage measuring transmission through a DNH at the instance of trapping at approximately 13 s.

Here, we use the cooling stage to lower the temperature to 14±2°C at the position of the DNH and wait for stabilization (details in Methods section), then turn on the laser power

to 20 mW (as measured before the objective, with a transmission of 75% at 850 nm for the objective) and reduce the power in steps of 2 mW, which corresponds to a local temperature decrease of 1°C considering the objective losses and laser heating.[33] We did not simply change the temperature of the stage because it resulted in changing the optical path length (e.g., through thermal changes to refractive index of the liquid in solution) and thereby required realignment at each new set temperature. Therefore, we opted to vary the laser power to heat locally and not require overall realignment of the setup for each temperature value.

Methods

Thermal Stage

The cooling stage was 3D-printed to be compatible with the ThorLabs "MAX3SLH-Microscopy Slide Holder" in the optical tweezer kit, while adding a position for the thermal reservoir. The stage was made of polyethylene terephthalate glycol to minimize thermal expansion. We used a three peltier thermoelectric cooler stack connected electrically in parallel (TEC1-12704K10, TECE-12704K10, CP2020405H), which were controlled using a temperature controller (ILX Lightwave LDT-5910B). To serve as a heat sink, a copper cylinder with a vented brass cap containing a palm and paraffin wax blend (Make Market) was held flush to the largest peltier cooler. A copper connection bridged the smallest peltier cooler to the top of the sample (on the glass side, not the gold side), and a thermistor (Amphenol Sensors, TH310J39G) was glued at this interface for control feedback. Thermal grease was used between each element. Additional temperature probes were placed on the bottom slide adjacent to the microwell to obtain the temperature at the proximal and distal ends and thereby estimate the temperature at the location of the DNH.

Nanofabrication

Samples were prepared in a manner similar to our past approach.[37,38] A glass microslide (Fisherbrand 12-550C, $76\times25.4\times1.0$ mm^3) was cut into thirds by scribing with a diamond tip and cleaving. The sample was cleaned with 99% ethanol and dried with nitrogen gas. Slides were sonicated in ethanol for ten minutes, then rinsed with acetone, deionized water, and ethanol with drying between each step. A solution of 1:100 of 300 nm diameter polystyrene beads (Sigma-Aldrich, MFCD00131491 LB3) and 99% ethanol was distributed evenly on the glass slides and left overnight to evaporate the ethanol to form a mask comprising the beads in randomized formation, including dimers. The slides were plasma etched for 170 s (Harrick PDC plasma cleaner) to control cusp size, then subject to sputtering of 7 nm titanium followed by 70 nm gold (Mantis QUBE system). Beads were removed by adhesive tape after ten minutes of sonication in ethanol. Samples were cleaned by rinsing with ethanol and nitrogen gas drying, cut into quarters using a diamond scribe, then cleaned again. SEM imaging (Hitachi S-4800) showed DNHs were on average 471 nm across and their cusp size was 33±3 nm.

BSA Sample Preparation

9.4 μL of a 10 mg/mL suspension of BSA (Sigma-Aldrich, MWGF70-1KT) in 10 μM PBS was added to a microwell created by placing an 0.1 mm thick image spacer (Grace BioLabs, GBL-654008-100EA) onto a glass slide-0 (Globe Scientific Inc., 1419-10). The solution was sealed with the DNH sample with the gold-face down.

Temperature Controlled Trapping

Prior to trapping, we measured the temperature at the copper plate 1 mm of glass away from the gold film (8°C) and at the cover slip at the proximal and distal ends (average 15.5°C). Based on these values, we estimate that the temperature at the center of the sample where

the DNH was located was 14±1°C. Based on our previous work,[33] the laser increased the local temperature by 0.6°C/mW at the sample, and the power was measured before the objective and a power loss of 25% at the 850 nm wavelength was taken from the specification sheet.

We waited 14 minutes to allow the temperature to stabilize. The laser was then turned on and aligned to the DNH of the sample. The 850 nm laser (Eagleyard dfb-0852-00050-BFY02-0002) was collimated and passed through a linear polarizer and half waveplate then expanded before entering a 100× oil immersion microscope objective (1.25 NA, Nikon CFI E Plan Achromat 100× Oil). Once through the DNH, light was collected by a 10× microscope objective (0.25NA, Olympus Plan N 10×/0.25 Fn22) then measured using an APD (Thorlabs, APD110A) and digitized with a data acquisition module (Advantech, USB-4711A). The DNH was visualized using a camera to assist in alignment. Once the protein trapped (seen by a jump in the APD voltage and increased noise), the signal was observed for 16 mins and the laser current was reduced by 10 mA intervals while the temperature was maintained to within ±0.3°C by the controller.

Results and Discussion

Figure 2 shows the transitions between the N and F states observed in the time-series of the APD voltage for different temperatures. The N state is more compact and shows less scattering (lower APD voltage) than the F state (higher APD voltage).[33] We also ran experiments at higher temperatures and saw the E state; however, we do not report on that here since it was covered in our previous work.[33] The data was acquired at 10 kS/s, and a simple 100 point average was used to reduce noise. The time-series data was binned by the normalized voltage, with 50 bins over the range covering both N and F states. The binning was carried out over a 10 second window and was done on the 100 point averaged data. The total time for the data presented was 19.5 minutes; however, we repeated the experiment at 6 different set-point temperatures, three at lower temperature values, where the range of

temperatures overlapped with the presented data and showed the same behavior.

Figure 2 also shows the corresponding probability density functions extracted from the time series data, with a double Gaussian fit (measuring the changes in the transmission intensity with conformational changes of BSA). From the area under each Gaussian (A_N, A_F), the time spent in each state was found. In our past work, we corrected the probability density by deconvolution to account for translational and other fluctuations.[33] This was required to accurately represent the energy landscape; however, here we are interested in the relative occupancy of each state and so the simple Gaussian fitting procedure is suitable. Once the Gaussian fits were found, we added the mean values to the time series plots as horizontal dashed lines to show clearly the high and low voltage states.

Figure 3 shows the natural logarithm of the ratio between the time spent in each state. This is described by transition state theory with the Arrhenius equation:

$$\frac{A_F}{A_N} \propto e^{-\frac{\Delta G_{NF}}{k_B T}} \tag{2}$$

where $A_{F,N}$ is the area (time) of states N and F, ΔG_{NF} is the change in the Gibbs free energy when transitioning between these states, k_B is the Boltzmann constant and T is the temperature. Using this Arrhenius dependence, the natural logarithm of the ratio of areas gives the change in Gibbs free energy when transitioning between the N and F conformations, in units of k_BT (and to within a constant offset). A maximum is seen for 21$\pm$1°C. We interpret this as the maximum stability point for the N state with respect to the F state.

Past circular dichroism measurements suggested that there is a transition at around 30°C (in 5°C steps), where they interpreted the data as α helix contributions being replaced with β sheet contributions.[36] This 30°C value is neither comparable to the 21°C maximum stability of the N with respect to F forms, or the 36°C maximum stability expected from Gibbs-Helmoltz theory, or the 39°C maximum stability of the E with respect to F state found from our past work.[33] We do note that above 25°C, we have observed that the E form starts to

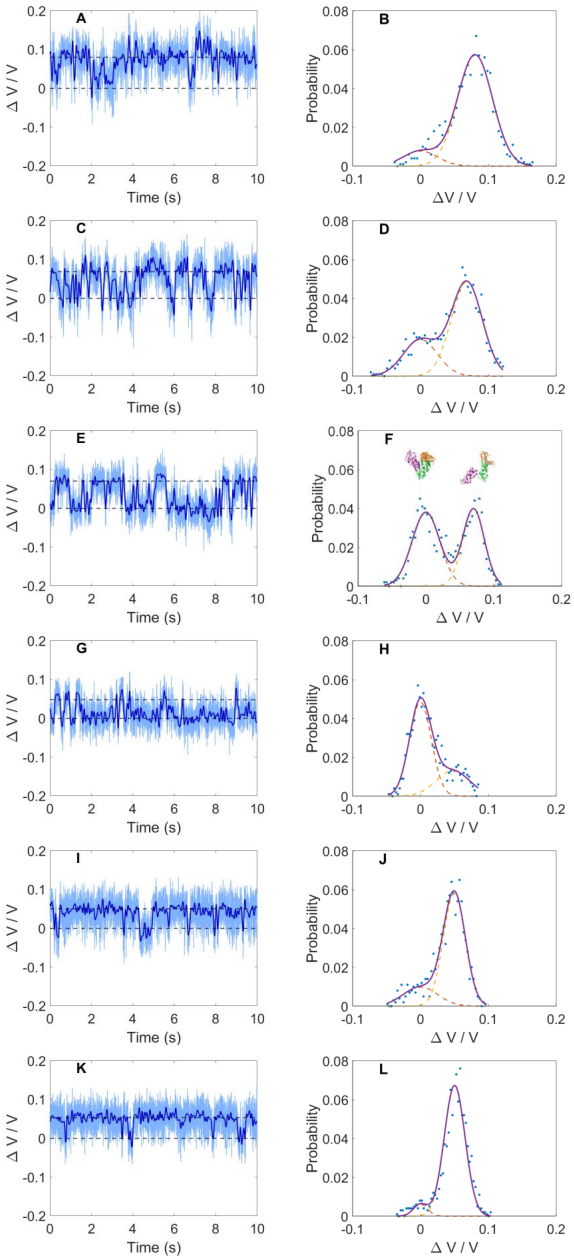

Figure 2: a) APD voltage measuring transmission through aperture with BSA trapped and corresponding PDFs at (a,b) 18±1°C, (c,d) 19±1°C, (e,f) 20±1°C, (g,h) 21±1°C, (i, j) 22±1°C, (k,l) 23±1°C. The N and F levels are indicated by dashed horizontal lines taken from mean of Gaussian fits. The voltages were normalized to allow comparison at different temperatures by dividing through by the voltage of the N-state level (0.4089 V, 0.5045 V, 0.5735 V, 0.6981 V, 0.8134 V, and 0.9037 V for 19±1°C, 20±1°C, 21±1°C, 22±1°C, and 23±1°C). f) Shows schematic of conformations of BSA as inset.

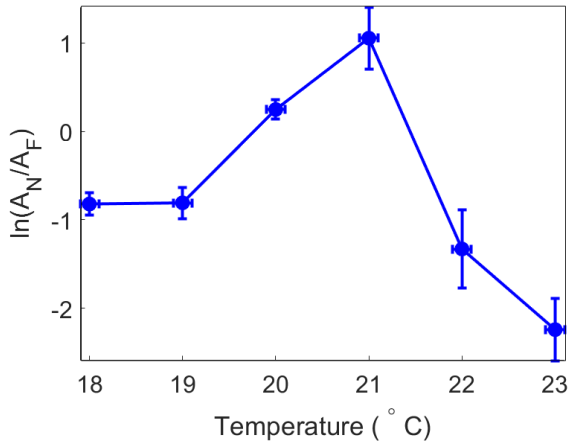

Figure 3: Natural logarithm of ratio of time in each state for N and F states of BSA for different temperatures. A maximum is found at 21 ± 1°C, which is interpreted as the maximum stability temperature for the compact N form. The error bar in the temperature was from the measured fluctuations at the thermistor and the error bar in the vertical axis was from uncertainties found by the Gaussian fitting procedure.

appear, so we believe their finding is showing the onset of the E state. A recent work has explored this further with changes in pH and indeed showed that when the E form appeared, β-rich spectra were seen.[39]

While it is tempting to suggest that the maximum of Fig. 3 is the absolute maximum stability temperature, the picture is more complicated since there are different conformations. The stability found here is relative to other states. The absolute stability would require knowing the Gibbs free energy of each state, not only the relative values. The Gibbs-Helmholtz model compares folded to unfolded proteins in a two state system, and it is not clear how that can be applied to the many stable conformations that are present in BSA at different temperatures. Clearly there is room to develop models to better understand this behavior. If we could obtain the absolute Gibbs free energy, more insight into the dynamics of BSA would be possible. For example, the Gibbs free energy has been related to the Soret coefficient for thermophoretic diffusion, where:[40]

$$S = \frac{1}{k_B T} \frac{dG}{dT} \tag{3}$$

Based on that theory, where the Soret coefficient transitions from negative (thermophilic) to positive (thermophobic), there should be a maximum in the Gibbs free energy. By measuring the Soret coefficient as a function of temperature it may be possible to extract the maximum stability point. The thermophoretic contribution to trapping has been explored with NOTs by changing the surfactant;[18] however, it is difficult to extract the absolute thermophoretic contribution with that approach since both the trap stiffness and laser heating (linked to thermophoretic force) depend on the laser power.

Conclusions

In summary, we have investigated the low temperature stability of BSA by adding a thermal stage. With this temperature control, the NOT setup able to trap single unmodified proteins in solution and observe their conformational changes in real time. We found a maximum in the N state stability with respect to the F state, occurring at 21°C. The thermal stage used phase transition materials to effectively remove heat while not requiring liquid cooling or fans that could introduce vibrations to the setup. The natural function of proteins often involves conformational changes and by introducing a thermal cooling stage into our setup, we have enabled the study of proteins and their interactions in the range where proteins are typically maximally stable.[41] In the future, this may be applied to the study the affect of temperature on protein interactions with small molecules,[42] changes in environment[22] and the impact of mutation on the conformational stability.[43]

Acknowledgement

The authors acknowledge support from NSERC Discovery Grant RGPIN-2023-04-18.

References

(1) Zijlstra, P.; Paulo, P. M.; Orrit, M. Optical detection of single non-absorbing molecules using the surface plasmon resonance of a gold nanorod. *Nat. Nanotechnol.* **2012**, *7*, 379–382.

(2) Pang, Y.; Gordon, R. Optical trapping of a single protein. *Nano Lett.* **2012**, *12*, 402–406.

(3) Dantham, V. R.; Holler, S.; Barbre, C.; Keng, D.; Kolchenko, V.; Arnold, S. Label-free detection of single protein using a nanoplasmonic-photonic hybrid microcavity. *Nano Lett.* **2013**, *13*, 3347–3351.

(4) Liang, F.; Guo, Y.; Hou, S.; Quan, Q. Photonic-plasmonic hybrid single-molecule nanosensor measures the effect of fluorescent labels on DNA-protein dynamics. *Sci. Adv.* **2017**, *3*, e1602991.

(5) Hogan, N. J.; Urban, A. S.; Ayala-Orozco, C.; Pimpinelli, A.; Nordlander, P.; Halas, N. J. Nanoparticles heat through light localization. *Nano Lett.* **2014**, *14*, 4640–4645.

(6) Dongare, P.; Alabastri, A.; Neumann, O.; Nordlander, P.; Halas, N. J. Solar thermal desalination as a nonlinear optical process. *Proc. Natl. Acad. Sci. U.S.A.*. **2019**, *116*, 13182–13187.

(7) Dongare, P. D.; Zhao, Y.; Renard, D.; Yang, J.; Neumann, O.; Metz, J.; Yuan, L.; Alabastri, A.; Nordlander, P.; Halas, N. J. A 3D Plasmonic Antenna-Reactor for Nanoscale Thermal Hotspots and Gradients. *ACS Nano* **2021**, *15*, 8761–8769.

(8) Melentiev, P. N.; Afanasiev, A. E.; Kuzin, A. S., A. A.and Baturin; Balykin, V. I. Giant optical nonlinearity of a single plasmonic nanostructure. *Opt. Express* **2013**, *21*, 13896–13905.

(9) Juan, M. L.; Gordon, R.; Pang, Y.; Eftekhari, F.; Quidant, R. Self-induced back-action optical trapping of dielectric nanoparticles. *Nat. Phys.* **2009**, *5*, 915–919.

(10) Pang, Y.; Gordon, R. Optical trapping of 12 nm Dielectric Spheres Using Double-Nanoholes in a Gold Film. *Nano Lett.* **2011**, *11*, 3763–3767.

(11) Berthelot, J.; Aćimović, S. S.; Juan, M. L.; Kreuzer, M. P.; Renger, J.; Quidant, R. Three-dimensional manipulation with scanning near-field optical nanotweezers. *Nat. Nanotechnol.* **2014**, *9*, 295–299.

(12) Kerman, S.; Chen, C.; Li, Y.; Van Roy, W.; Lagae, L.; Van Dorpe, P. Raman fingerprinting of single dielectric nanoparticles in plasmonic nanopores. *Nanoscale* **2015**, *7*, 18612–18618.

(13) Jensen, R. A.; Huang, I.-C.; Chen, O.; Choy, J. T.; Bischof, T. S.; Loncar, M.; Bawendi, M. G. Optical trapping and Two-Photon Excitation of Colloidal Quantum Dots using Bowtie Apertures. *ACS Photonics* **2016**, *3*, 423–427.

(14) Raza, M. U.; Peri, S. S. S.; Ma, L.-C.; Iqbal, S. M.; Alexandrakis, G. Self-induced back action actuated nanopore electrophoresis (SANE). *Nanotechnology* **2018**, *29*, 435501.

(15) Yoo, D.; Gurunatha, K. L.; Choi, H.-K.; Mohr, D. A.; Ertsgaard, C. T.; Gordon, R.; Oh, S.-H. Low-Power Optical Trapping of Nanoparticles and Proteins with Resonant Coaxial Nanoaperture Using 10 nm Gap. *Nano Lett.* **2018**, *18*, 3637–3642.

(16) Kotnala, A.; Kollipara, P. S.; Li, J.; Zheng, Y. Overcoming Diffusion-Limited Trapping in Nanoaperture Tweezers Using Opto-Thermal-Induced Flow. *Nano Lett.* **2019**, *20*, 768–779.

(17) Yoon, S. J.; Song, D. I.; Lee, J.; Kim, M.-K.; Lee, Y.-H.; Kim, C.-K. Hopping of single nanoparticles trapped in a plasmonic double-well potential. *J. Nanophotonics* **2020**, *9*, 4729–4735.

(18) Jiang, Q.; Rogez, B.; Claude, J.-B.; Baffou, G.; Wenger, J. Quantifying the Role of the Surfactant and the Thermophoretic Force in Plasmonic Nano-optical Trapping. *Nano Lett.* **2020**, *20*, 8811–8817.

(19) Kotsifaki, D. G.; Truong, V. G.; Nic Chormaic, S. Fano-Resonant, Asymmetric, Metamaterial-Assisted Tweezers for Single Nanoparticle Trapping. *Nano Lett.* **2020**, *20*, 3388–3395.

(20) Li, N.; Cadusch, J.; Liu, A.; Barlow, A. J.; Roberts, A.; Crozier, K. B. Algorithm-Designed Plasmonic Nanotweezers: Quantitative Comparison by Theory, Cathodoluminescence, and Nanoparticle Trapping. *Adv. Opt. Mater.* **2021**, *9*, 2100758.

(21) Yang, W.; van Dijk, M.; Primavera, C.; Dekker, C. FIB-milled plasmonic nanoapertures allow for long trapping times of individual proteins. *iScience* **2021**, *24*, 103237.

(22) Ying, C.; Karakaci, E.; Bermudez-Urena, E.; Ianiro, A.; Foster, C.; Awasthi, S.; Guha, A.; Bryan, L.; List, J.; Balog, S.; Acuna, G. P.; Gordon, R.; Mayer, M. Watching Single Unmodified Enzymes at Work. 2021; arXiv.2107.06407 (physics.bio-ph), July 13 2021, available at `https://arxiv.org/abs/2107.06407`, accessed 2024-11-21.

(23) Wu, B.; Lou, Y.; Wu, D.; Min, Q.; Wan, X.; Zhang, H.; Yu, Y.; Ma, J.; Si, G.; Pang, Y. Directivity-Enhanced Detection of a Single Nanoparticle Using a Plasmonic Slot Antenna. *Nano Lett.* **2022**, *22*, 2374–2380.

(24) Hong, C.; Ndukaife, J. C. Scalable trapping of single nanosized extracellular vesicles using plasmonics. *Nat. Commun.* **2023**, *14*, 4801.

(25) Yousefi, A.; Ying, C.; Parmenter, C. D.; Assadipapari, M.; Sanderson, G.; Zheng, Z.; Xu, L.; Zargarbashi, S.; Hickman, G. J.; Cousins, R. B.; Mellor, C. J.; Mayer, M.; Rahmani, M. Optical Monitoring of In Situ Iron Loading into Single, Native Ferritin Proteins. *Nano Lett.* **2023**, *23*, 3251–3258.

(26) Yousefi, A.; Zheng, Z.; Zargarbashi, S.; Assadipapari, M.; Hickman, G. J.; Parmenter, C. D.; Bueno-Alejo, C. J.; Sanderson, G.; Craske, D.; Xu, L.; Perry, C. C.; Rahmani, M.; Ying, C. Structural Flexibility and Disassembly Kinetics of Single Ferritin Molecules Using Optical Nanotweezers. *ACS Nano* **2024**, *18*, 15617–15626.

(27) Ma, J.; Zhang, H.; Lou, Y.; Min, Q.; Wu, D.; Wang, Y.; Pang, Y. Deterministic Assembly of Single-Emitter Plasmonic Antenna for Ultrahigh Photoluminescence Enhancement. *Nano Lett.* **2024**, *24*, 12605, 12611.

(28) Xu, Z.; Song, W.; Crozier, K. B. Direct Particle Tracking Observation and Brownian Dynamics Simulations of a Single Nanoparticle Optically Trapped by a Plasmonic Nanoaperture. *ACS Photonics* **2018**, *5*, 2850–2859.

(29) Verschueren, D.; Shi, X.; Dekker, C. Nano-Optical Tweezing of Single Proteins in Plasmonic Nanopores. *Small Methods* **2019**, *3*, 1800465.

(30) Jiang, Q.; Rogez, B.; Claude, J.-B.; Baffou, G.; Wenger, J. Temperature Measurement in Plasmonic Nanoapertures used for Optical Trapping. *ACS Photonics* **2019**, *6*, 1763–1773.

(31) Jiang, Q.; Rogez, B.; Claude, J.-B.; Moreau, A.; Lumeau, J.; Baffou, G.; Wenger, J. Adhesion layer influence on controlling the local temperature in plasmonic gold nanoholes. *Nanoscale* **2020**, *12*, 2524–2531.

(32) Toodeshki, E. H.; Frencken, A. L.; van Veggel, F. C.; Gordon, R. Thermometric Analysis of Nanoaperture-Trapped Erbium-Containing Nanocrystals. *ACS Photonics* **2024**, *11*, 1390–1395.

(33) Peters, M.; Zhao, T.; George, S.; Truong, V. G.; Nic Chormaic, S.; Ying, C.; Nome, R. A.; Gordon, R. Energy landscape of conformational changes for a single unmodified protein. *npj Biosensing* **2024**, *1*, 14.

(34) Pal, S.; Pyne, P.; Samanta, N.; Ebbinghaus, S.; Mitra, R. K. Thermal stability modulation of the native and chemically-unfolded state of bovine serum albumin by amino acids. *Phys. Chem. Chem. Phys.* **2020**, *22*, 179–188.

(35) Becktel, W. J.; Schellman, J. A. Protein stability curves. *Biopolymers* **1987**, *26*, 1859–1877.

(36) Takeda, K.; Wada, A.; Yamamoto, K.; Moriyama, Y.; Aoki, K. Conformational change of bovine serum albumin by heat treatment. *J. Protein Chem.* **1989**, *8*, 653–659.

(37) Ravindranath, A. L.; Shariatdoust, M. S.; Mathew, S.; Gordon, R. Colloidal lithography double-nanohole optical trapping of nanoparticles and proteins. *Opt. Express* **2019**, *27*, 16184–16194.

(38) Hajisalem, G.; Babaei, E.; Dobinson, M.; Iwamoto, S.; Sharifi, Z.; Eby, J.; Synakewicz, M.; Itzhaki, L. S.; Gordon, R. Accessible high-performance double nanohole tweezers. *Opt. Express* **2022**, *30*, 3760–3769.

(39) de Resende, L. F. T.; Basilio, F. C.; Alliprandini Filho, P.; Therézio, E. M.; Silva, R. A.; Oliveira Jr, O. N.; Marletta, A.; Campana, P. T. Revisiting the conformational transition model for the pH dependence of BSA structure using photoluminescence, circular dichroism, and ellipsometric Raman spectroscopy. *Int. J. Biol. Macromol.* **2024**, *259*, 129142.

(40) Eastman, E. D. Theory of the Soret effect. *J. Am. Chem. Soc.* **1928**, *50*, 283–291.

(41) Razvi, A.; Scholtz, J. M. Lessons in stability from thermophilic proteins. *Protein Sci.* **2006**, *15*, 1569–1578.

(42) Al Balushi, A. A.; Gordon, R. Label-Free Free-Solution Single-Molecule Protein–Small Molecule Interaction Observed by Double-Nanohole Plasmonic Trapping. *ACS Photonics* **2014**, *1*, 389–393.

(43) Banerjee, A.; Mathew, S.; Naqvi, M. M.; Yilmaz, S. Z.; Zacharopoulou, M.; Doruker, P.; Kumita, J. R.; Yang, S.-H.; Gur, M.; Itzhaki, L. S.; Gordon, R. Influence of point mutations on PR65 conformational adaptability: Insights from molecular simulations and nanoaperture optical tweezers. *Sci. Adv.* **2024**, *10*, eadn2208.

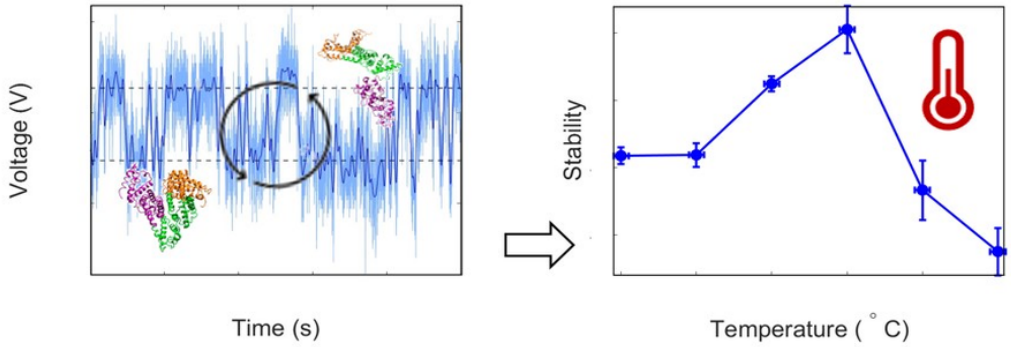

TOC graphic.

TOC Graphic

The TOC image is included above.